JOURNAL OF MATERIALS SCIENCE 29 (1994) 1203–1212

Influence of hydrogen charging on mechanical properties of gas tungsten arc weldments of aluminium-lithium alloy 8090

A. RAVINDRA*, AMIT BANDYOPADHYAY†, E. S. DWARAKADASA
Structure Property Correlation Group, Department of Metallurgy, Indian Institute of Science, Bangalore 560 012, India

T. S. SRIVATSAN
Department of Mechanical Engineering, The University of Akron, Akron, OH 44325, USA

The effect of hydrogen charging on the mechanical properties of gas tungsten arc welds (GTAW) of aluminium–lithium alloy 8090 (2 mm thick rolled sheets) was studied using cathodic hydrogen charging. To stimulate an increased amount of hydrogen into welds, the charging current density was increased through a galvanostatic circuit. The deleterious effect of hydrogen on ductility is documented in terms of degradation in tensile ductility (reduction in area and elongation-to-failure). Microscopic analysis was performed to characterize the microstructure and grain morphology of the weldments. Hardness measurements revealed an increase in hardness of the charged welds over the uncharged counterpart. Scanning electron microscopy observations of uncharged welds revealed a mixed mode failure with predominantly ductile rupture. Although, the charged welds exhibited a near similar mode of failure to that of the uncharged welds, extensive planar slip deformation was observed near the outer surface of the uncharged welds. The change in fracture mode from the outer surface to the central portion of the charged welds is attributed to intrinsic differences in hydrogen densities. An attempt has been made to rationalize the role of hydrogen on tensile properties and quasi-static fracture behaviour of the GTAW welds.

1. Introduction

A growing need to save fuel and the driving force to decrease operational cost of an aircraft, by decreasing structural weight, has focused considerable scientific and technological interest in the development of a spectrum of lightweight materials. In response to this critical need, several materials are being developed with the objective of replacing the conventional alloys currently being used in the aerospace industry. As a result, metal-matrix composites, polymer-matrix composites, ceramic-matrix composites and lightweight lithium-containing aluminium alloys have emerged as attractive and competitive alternatives for the conventional materials used in aerospace applications. Among these, the lithium-containing aluminium alloys potentially provide excellent combinations of reduced density (8%–10% lower than that of conventional aluminium alloys), high strength-to-weight ratio, improved stiffness (10%–12% higher), excellent formability, fairly good resistance to both exfoliation corrosion and stress corrosion cracking over other 2XXX and 7XXX series aluminium alloys. An overview of this development and details pertaining to research can be found in the proceedings of various conferences [1–6]. The many advantages they have to offer make them appear to be a cost-effective and an ideal candidate for weight-critical and stiffness-critical structures for military, space and commercial applications. In addition to these attractive properties, concurrent improvements in manufacturing and/or fabrication methods of these alloys through powder metallurgy (PM), rapid solidification techniques have taken place [2–6]. Consequently, these alloys are increasingly being recognized as candidate structural materials for a variety of aircraft applications.

The economic benefits associated with the direct substitution and use of these alloys for conventional aerospace alloys resulted in the resurrection of considerable technological interest in developing new alloys that offered improved mechanical properties and corrosion resistance [5–13]. An extensive research effort was directed at optimizing alloy compositions while concurrently developing casting, fabrication and heat-treatment procedures to give a balance of properties equal to or better than those of conventional alloys. This led to the emergence of a range of ingot metallurgy alloys belonging to the Al–Li–Cu–Zr and Al–Li–Cu–Mg–Zr systems, in plate, sheet, billet and extrusion forms. The major commercial alloys from these systems are registered with the Aluminium

* *Present address*: Department of Mechanical Engineering, The University of Akron, Akron, OH 44325, USA.
† *Present address*: Department of Mechanical Engineering, The University of Texas, Arlington, USA.

0022–2461

Association as alloy 2090 (ALCOA, USA), alloy 2091 (Cegedur Pechiney, Voreppe, France), alloy 8090 (ALCAN International Ltd, Banbury, UK), and X2095 (formerly Weldalite™ 049; Reynolds Metals Company, Richmond, USA). Alloys 2090 and 8091 are considered as attractive high-strength alternatives for the Al–Cu–Zn–Mg (7XXX series) alloys, whereas, alloys 8090 and 2091 are projected as attractive alternatives for medium-strength and damage-tolerant applications replacing the existing Al–Cu–Mg (2XXX series) aluminium alloys; and X2095 for structural applications requiring weldability and high strength at cryogenic temperatures [13]. Primary disadvantages in acceptance and use of these alloys were anisotropy of properties, low short-transverse properties of thick-section products, lack of manufacturing experience in the aerospace industry, lack of design allowables and above all cost, somewhere in the neighbourhood of four times the cost of the aluminium alloys they were designed to replace [14].

Complex contour and configuration of modern aircraft structures has necessitated the need to develop joining methods that would extend the range of applications for these alloys and to improve the overall performance, durability and damage tolerance. Fabrication by welding is comparatively more economical and convenient than conventional mechanical fastening [15]. Furthermore, welding offers several advantages such as (a) joining of both thin and thick sections, (b) high rate of production, and (c) automation and high joint efficiency. Over the years, several studies have been carried out to evaluate the weldability aspects of the conventional aerospace aluminium alloys belonging to the 2XXX (Al–Cu–Mg) and 7XXX (Al–Cu–Zn–Mg) series. Although these studies have met with appreciable degree of success, a comprehensive understanding of metallurgical aspects and influences on the weldability of the newer generation aluminium–lithium alloys is required, in order to exploit the attractive advantages of these materials.

A comprehensive review of the published literature on weldable lithium-containing aluminium alloys is provided elsewhere [16]. More recently, Molian and co-workers [17–19] evaluated the weldability of Al–Li alloy 2090 (Al–Li–Cu) using a laser-welding technique and concluded that laser welding offered several advantages, including high joint efficiencies over conventional fusion-welding processes. Edwards and Stoneham [20] evaluated the weldability of Alloy 8090 (Al–Li–Cu–Mg–Zr) using the gas tungsten arc welding (GTAW) process, while Le Poac *et al.* [21] evaluated the mechanical properties of electron-beam welds of alloy 8090. Kramer *et al.* [22] documented the fusion-welding characteristics of alloy 8090 using gas tungsten arc welding technique. All of these studies on the Al–Li–Cu–Mg alloy 8090 revealed it to have satisfactory weldability.

Several studies, in recent years, have found the aluminium–lithium alloys to be environment sensitive and susceptible to hydrogen embrittlement [23–26]. Hydrogen absorption in these alloys occurs either during environment-assisted corrosion and/or during thermal treatments such as welding and heat treatment, leading to moisture entrapment. Absorption of hydrogen in these alloys was found to have a detrimental influence on mechanical and corrosion properties. The loss of ductility due to hydrogen embrittlement was ascribed to the formation and presence of soluble hydrides of either lithium (LiH) or aluminium and lithium (Li_3AlH_6) [27]. Significant improvements in tensile ductility (expressed as elongation-to-failure) and toughness (expressed as ratio of notched tensile strength to unnotched tensile strength) with concurrent decrease in yield strength could be achieved by reducing the hydrogen content from 45 p.p.m. to 14 p.p.m. [27]. A review of hydrogen effects on the deformation behaviour of these alloys is reported elsewhere [28]. However, there still exists no conclusive evidence for precisely outlining the influence and role of hydrogen on the deformation behaviour of these alloys.

In view of the above studies and results reported in the published literature on alloy 8090, the present investigation on weldability of the alloy was undertaken. While an extensive study on weldability of alloy 8090 has been completed, only aspects pertaining to the effect of hydrogen charging on gas tungsten arc welds of the alloy are reported and discussed in this paper.

2. Experimental procedure

2.1. Material

The alloy selected for this investigation was aluminium–lithium alloy 8090. The alloy was provided by Alcan International Ltd (Banbury, UK), in the T6 temper. The as-received material was in the form of large rolled sheets, 2 mm thick. The nominal chemical composition of the alloy is given in Table I. Ambient temperature mechanical properties of the as-received (AR) material are summarized in Table II. The T6 temper involved solution heat treatment at 480 °C for 1 h, and quenching in water at ambient temperature. The as-quenched material was aged at 180 °C for 24 h.

The iron and silicon elements in the alloy are impurities. During ingot solidification and subsequent processing, these impurities precipitate as insoluble constituent phases, Al_3Fe and Al_7Cu_2Fe. Zirconium addition results in the formation of the metastable cubic Al_3Zr precipitates which are spherical in

TABLE I Chemical composition of Al–Li alloy 8090

Element	(wt %)
Li	2.2–2.7
Cu	1.0–1.6
Mg	0.6–0.16
Zr	0.04–0.16
Fe	0.3
Si	0.2
Cr	0.1
Mn	0.1
Zn	0.25
Ti	0.1
Al	Balance

TABLE II Mechanical properties of Al–Li alloy 8090-T6 in the as-received condition

Temper	Test direction	0.2% yield stress (MPa)	Ultimate tensile strength (MPa)	Elongation to failure (%)	Fracture toughness (MPa $m^{1/2}$)
T6 Typical	Longitudinal	365	455	4.0	80
	Transverse	375	465	7.5	60
T6 Spec min	Longitudinal	380	440	6.0	70
	Transverse	380	440	6.0	70

morphology and can effectively pin the grain and subgrain boundaries. The cubic Al_3Zr phase (β′), also known as dispersoid, has an $L1_2$ crystal structure and nucleates heterogeneously on dislocations and grain boundaries [29, 30]. The dispersoid particle is coherent with the aluminium matrix and aids in (i) retarding subgrain boundary coalescence, (ii) suppressing recrystallization, (iii) controlling grain growth, and (iv) stabilizing the subgrain structure [31]. Magnesium additions to ternary Al–Li–Cu alloy provides solid-solution strengthening and eliminates the formation of precipitate-free zones (PFZ's) through the precipitation of S″ and S′ (Al_2CuMg) phases near the grain boundaries [32].

2.2. Microstructural characterization

Metallographic samples were cut from the as-received sheet stock. The samples were mounted in cold-setting compound and wet ground on 320, 400 and 600 grit silicon carbide paper using water as lubricant and subsequently mechanically polished using an alumina-based polishing compound. Grain morphology was revealed using Keller's etchant. The specimens were etched for 60 s and examined in an optical microscope and photographed using standard bright-field technique.

2.3. Welding method

Rectangular plates, 300 mm × 60 mm (Fig. 1), with milled flat welding edges were used to obtain butt welds, using an argon gas shielded GTAW process. Commercially available filler wire AA5356 (Al–5%Mg; 1.8 mm diameter) was used with a current of 60 A. Before welding, the test plates were mechanically cleaned and chemically degreased. Occurrence of porosity in aluminium–lithium alloy welds have been attributed to the presence of absorbed hydrogen [33–35]. Therefore, in order to minimize porosity, the recommendation to remove the surface layer, to a depth of about 0.2–0.3 mm, prior to welding was observed.

Several surface removal methods ranging from grinding, milling, chemical milling and chemical etching in 30% NaOH solution, have been recommended for this purpose [36]. With this in mind, the welding edges were mechanically cleaned by polishing with silicon carbide-impregnated emery paper prior to welding. All plates were welded immediately after cleaning. Only radiographically acceptable quality welds were used for subsequent mechanical testing and analysis.

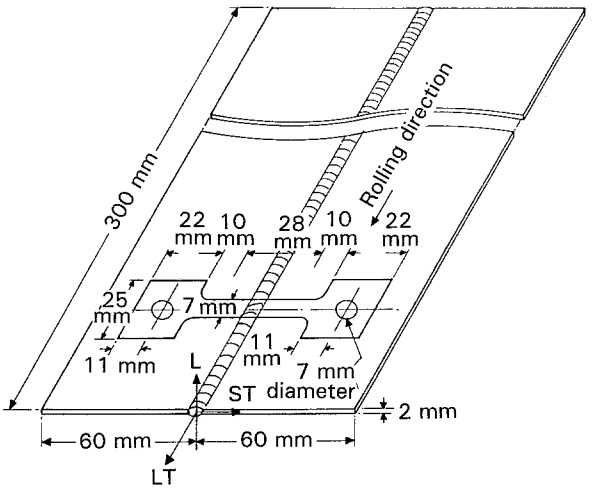

Figure 1 Schematic representation of a butt-welded joint showing the test region.

The transverse tensile test specimens (Fig. 1) were milled from these test welds.

Cathodic charging represents the most severe charging conditions and, hence, a deleterious influence on properties [34]. Therefore, the transverse tensile test specimens were cathodically charged to study the influence of hydrogen on properties of the weldments. The cathodic hydrogen charging was carried out using an increasing charging current density, ranging from 0.5–9.0 mA cm^{-2} and a galvanostatic circuit equipped with a d.c. power source. The cathodic hydrogen charging was carried out in a 3.5% NaCl aqueous solution, and the pH of the solution was monitored throughout charging. The cathodic hydrogen charging was carried out, for a period of 12 h, such that only the gauge section of the specimen was subjected to charging. After charging, all the specimens were cleaned using acetone and mechanically polished using 600 grit silicon carbide paper in order to remove the surface layer that undergoes dissolution. In an earlier investigation, these alloys were found to suffer from lithium depletion at the outer surface [37]. Mechanical polishing using silicon carbide-impregnated emery paper also aids in removing the lithium-depleted surface layer and this results in a specimen with "near" similar lithium concentration throughout the entire cross-section.

2.4. Mechanical testing

The effect of hydrogen charging on mechanical properties was studied by slow strain-rate tensile tests in

order to resolve the concurrent and competing influences of corrosive environment and mechanical deformation on overall performance of the weldment. The slow strain-rate tensile tests were carried out using a servohydraulic testing machine (Instron Model 8032), at a constant crosshead speed of 0.028 mm s^{-1} which corresponds to a nominal strain rate of 0.0001 s^{-1}. Vicker's hardness measurements and lithium analysis of the welds were also carried.

Fracture surfaces of the deformed tensile specimens were observed in a scanning electron microscope (SEM) in order to determine the predominant fracture mode and to characterize the fine-scale features on the fracture surface.

3. Results and discussion

3.1. Lithium analysis of the weld metal

Analysis of the weldments revealed the lithium content to have decreased in the weld metal. The lithium content in the parent alloy was 2.4% and only 1.7% in the weld metal. Dilution of lithium in the weld metal is ascribed to the fact that the filler material used does not contain any lithium.

3.2. Initial microstructure

A triplanar composite microstructure, illustrated in Fig. 2a, reveals the grain structure of the material in the three orthogonal directions; longitudinal (L), long-transverse (LT) and short-transverse (ST). The microstructure revealed elongated grains in the long-transverse and short-transverse directions, and "near" equiaxed grains in the longitudinal direction. Owing to the rolling operation, the grains in the longitudinal direction were elongated and had a "pancake" morphology. In recent years, investigators [38, 39] have shown alloy 8090 to exhibit a strong rolled texture, with deformation behaviour to be dependent on texture. The intrinsic influence of texture is to impart microstructural anisotropy. Consequently, reference to the rolling direction is important when mechanical properties are to be evaluated and reported. In a recent study, Ravindra *et al.* [40] found hydrogen embrittlement and susceptibility to stress corrosion cracking of the 8090 alloy were intrinsically related to orientation of the test specimen with respect to the rolling direction. Although the influence of grain morphology on environment-assisted fracture behaviour has been well understood and documented, detailed investigations are required to understand the synergistic influence of grain morphology and hydrogen charging on mechanical behaviour.

Microscopic analysis of the weld metal revealed predominantly equiaxed grains in all three orthogonal directions (Fig. 2b). This is typical of a cast microstructure. Dendritic growth observed in the weld metal revealed the grains near the root surface to be smaller in size in comparison with grains at the centre of the weld (Fig. 3). However, grains at the centre of the weld metal were non-uniform in size in comparison with the smaller, "near" equiaxed grains at and near the fusion line (Fig. 4). Both grain growth and coarsening in the weld metal region are influenced by the rate of cooling during solidification. Rapid cooling yields smaller grains while slow cooling results in larger grains. As a result of the higher rate of cooling at the root surface compared with the interior of the weld metal, the grains at and near the root surface were smaller in size. The influence of cooling rate on the grain size of aluminium–lithium alloy welds is documented elsewhere [41].

3.3. Mechanical properties

An increase in charging current density increases the amount of hydrogen generated in the specimen. Therefore, for a constant charging time and temperature, a pronounced influence of hydrogen on properties could be observed only at the higher current densities. The influence of hydrogen charging of alloy 8090 can be recognized when (a) ductility parameters are seriously impaired, and (b) there are intrinsic differences in hardness measurements. In the present case, the reduction in area (RA) and elongation-to-failure, ε_f, also decreased initially with an increase in charging current density. However, for current densities greater than 9 mA cm^{-2}, severe anodic dissolution occurred which made it impossible to realize the effect of the hydrogen charging beyond a current density of 9 mA cm^{-2}, severe anodic dissolution occurs causing, as a result, considerable pitting on the surface of the specimen. The pH of the aqueous solution was continuously monitored during cathodic hydrogen charg-

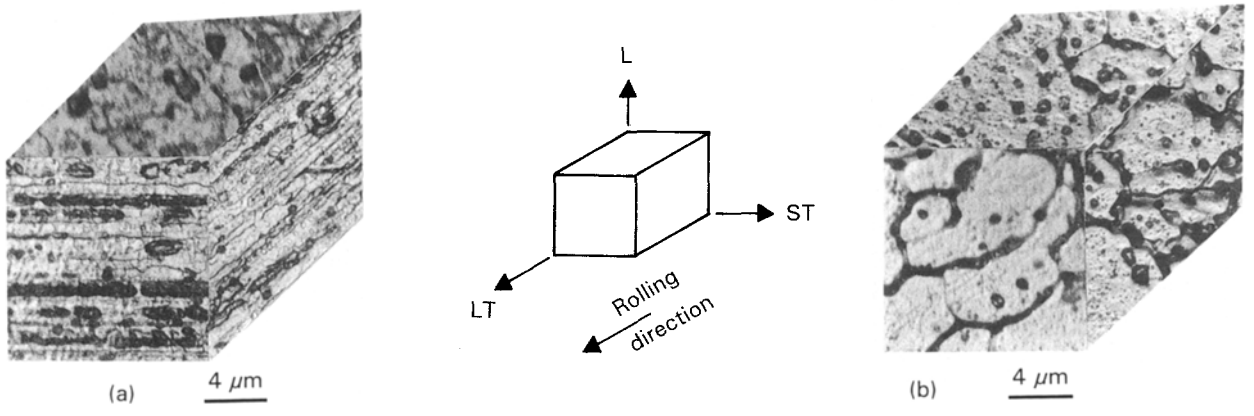

Figure 2 Optical microstructure of (a) alloy 8090-T6 illustrating a pancake grain morphology, (b) weld metal indicating typical cast structure.

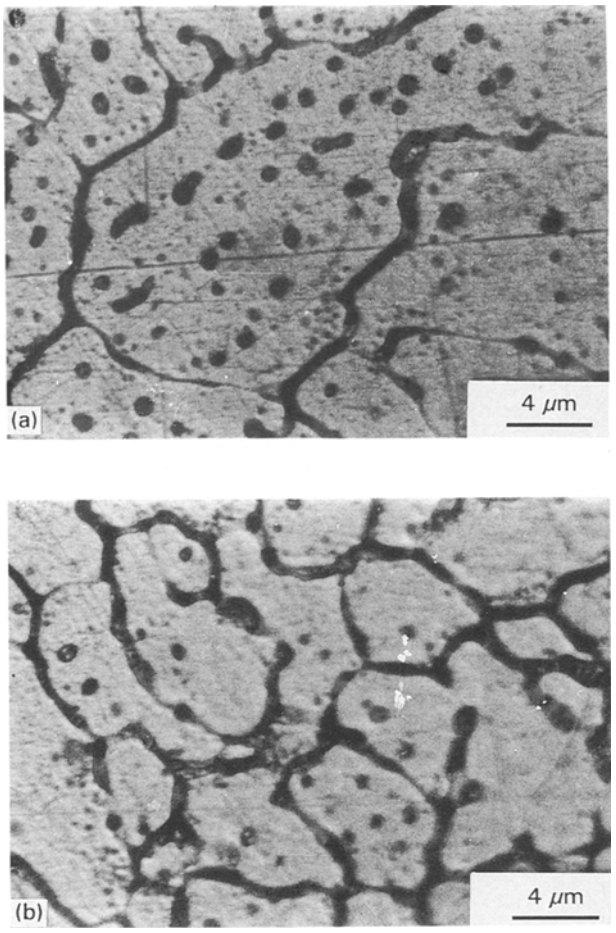

Figure 3 Optical microstructure of weld metal (a) at the centre of a weld, and (b) at the root surface of the weld.

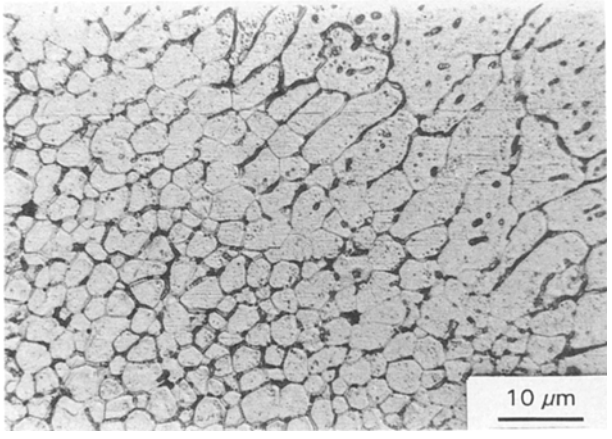

Figure 4 Optical microstructure of weld metal indicating equiaxed grains near the fusion line and oriented dendritic growth inside the weld.

ing. For hydrogen charging of each specimen, a fresh 3.5% NaCl solution was used and the charging environment was replaced once a change in solution pH was recorded. Inspite of these precautions, anodic dissolution was found to occur at and beyond current densities of 9 mA cm^{-2}. Therefore, hydrogen charging was limited to a current density of 9 mA cm^{-2}. The ultimate tensile strength (UTS) of all charged welds remained almost the same as that of the uncharged welds (Fig. 5). Failure of the welds occurred in the weld region. This indicates little to no influence of hydrogen charging on tensile strength of the welds, but a deleterious influence only on ductility.

The effect of hydrogen charging on the welds of alloy 8090 is recognized in terms of decrease in reduction in area (RA) and elongation-to-failure, ε_f, (Fig. 6). This is attributed to competing and synergistic influences of (a) the formation of hydrides of lithium in the weld metal as reported by Hill *et al.* [27], and (b) to the presence of gaseous hydrogen. During cathodic charging, nascent hydrogen (H) is generated in the test specimen, which is the anode. Compared to aluminium, hydrogen is smaller in diameter and readily diffuses into the matrix. The nascent hydrogen diffuses into the micropores present in the alloy, and forms hydrogen gas (H_2). With progressive diffusion of nascent hydrogen into the fine micropores, the gas pressure increases significantly. Apart from the formation and presence of high pressure hydrogen gas (H_2), in the micropores, nascent hydrogen also causes distortion of the aluminium lattice. The synergistic and competing influences of these two factors is to degrade the ductility of the quarternary Al–Li–Cu–Mg–Zr alloy 8090. However, the formation and presence of high-pressure hydrogen gas in these micropores had little influence on ultimate tensile strength of the welds, as revealed by the tensile tests.

In order to verify the formation of H_2 gas in the zones of microporosity of the welds, different specimens of alloy 8090, in the T851, were charged in a similar environment using identical charging current densities. Hardness measurements (Fig. 7a) were carried out on the charged samples of the alloy. To expel the hydrogen gas formed as a result of diffusion of nascent hydrogen (H), all of the charged specimens were degassed. Hardness measurements were performed across the thickness of the specimen. This is because diffusion of hydrogen occurs more at the surface of the specimen than at the centre. As a result, there is a higher hydrogen concentration at the specimen surface than at the centre. Intrinsic differences in hydrogen content in the specimen can be indirectly identified from hardness measurements. Hardness measurements across the thickness of the specimen revealed a higher hardness at the surface and an almost constant hardness at the centre. Thus, a hardness profile of the charged specimen provides a measure of the relative concentration of hydrogen in the charged specimen.

Following hardness measurements across the thickness, the charged specimens were degassed at 443 K for 1 h. After degassing at the elevated temperature, hardness of the degassed specimen was measured across the thickness (Fig. 7b) [42]. In order to minimize any contribution from ageing effects, the degassing temperature was chosen to be lower than the temperature at which the alloy was artificially aged. As a result, the precipitation kinetics was not appreciably influenced. Microscopic examination of the charged and degassed specimen failed to reveal any significant change in intrinsic microstructural features when compared to the charged and undegassed counterpart. During degassing care was exercised to

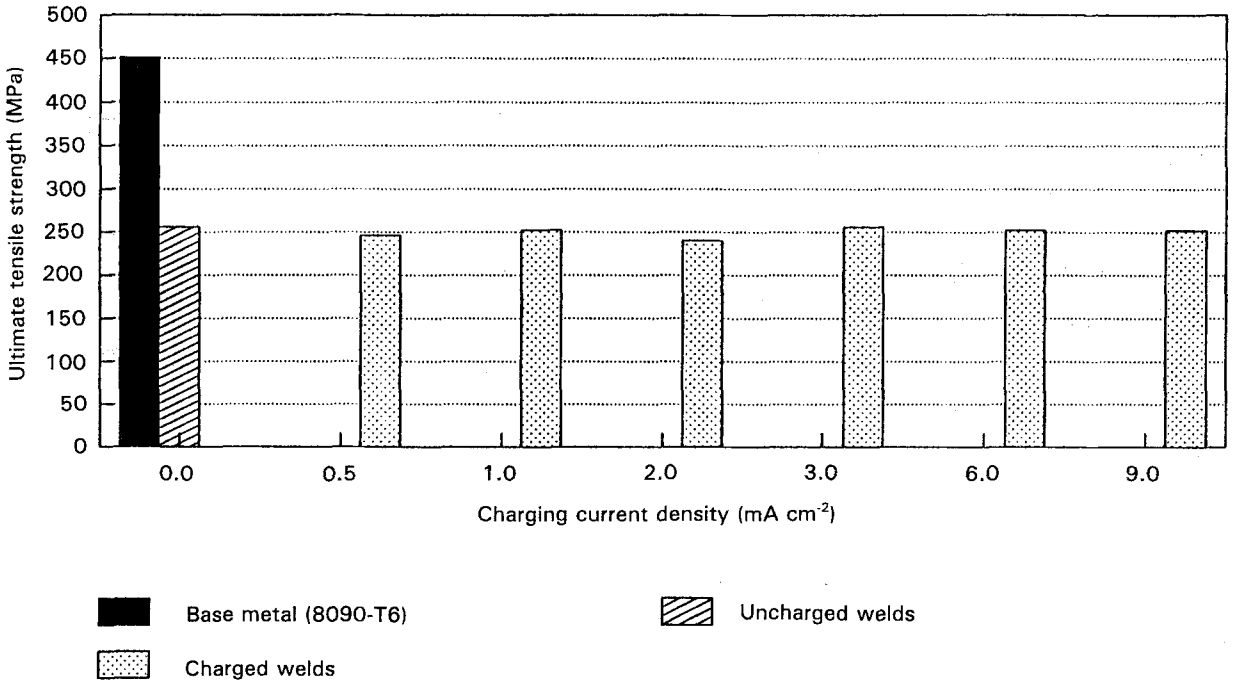

Figure 5 Transverse tensile strength of charged and uncharged gas tungsten arc welds (GTAW) of alloy 8090-T6.

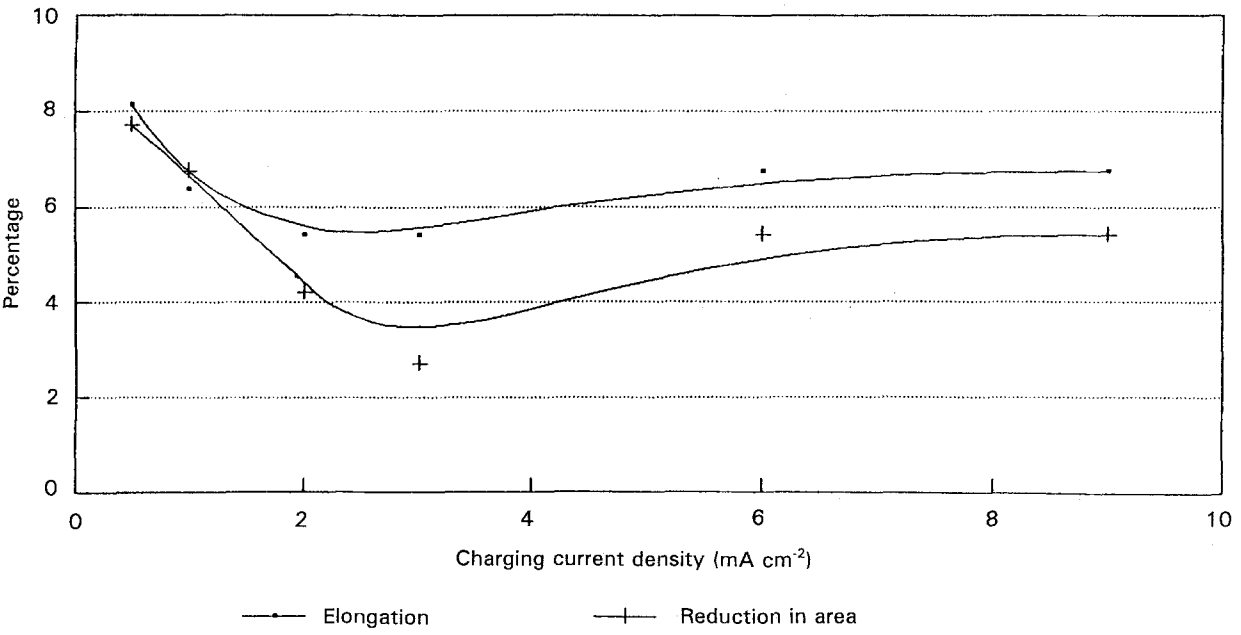

Figure 6 Influence of hydrogen charging on the ductility of gas tungsten arc welds (GTAW) of alloy 8090-T6.

ensure minimum damage to microstructure of the specimen.

Both uncharged and charged and degassed specimens indicated the same hardness values. Furthermore, the hardness profile of the charged and degassed specimens, across the thickness, was almost constant, unlike the hardness profile of the charged specimens which indicated an increase in hardness at the surface of the specimen. This observation is interesting and provides an appealing rationale for the formation and presence of hydrogen gas. Degassing the charged specimen has enabled the hydrogen content in the alloy to be decreased. This is well substantiated by hardness measurements across the thickness of the specimen (Fig. 7b). In addition, the hardness measurements indicate that even if stable hydrides of lithium are formed during cathodic charging, the degassing has helped in the removal of almost all of the hydrogen from the specimen. However, to ascertain this observation, measurements of the hydrogen density and hydrogen diffusion coefficients are required for both the charged specimens and the charged and degassed specimens. Because hydrogen density measurements could not be performed owing to lack of facilities, the observed phenomenon is interpreted and discussed with specific reference to hardness measurements. Furthermore, transmission electron microscopy observations are required for a thorough understanding

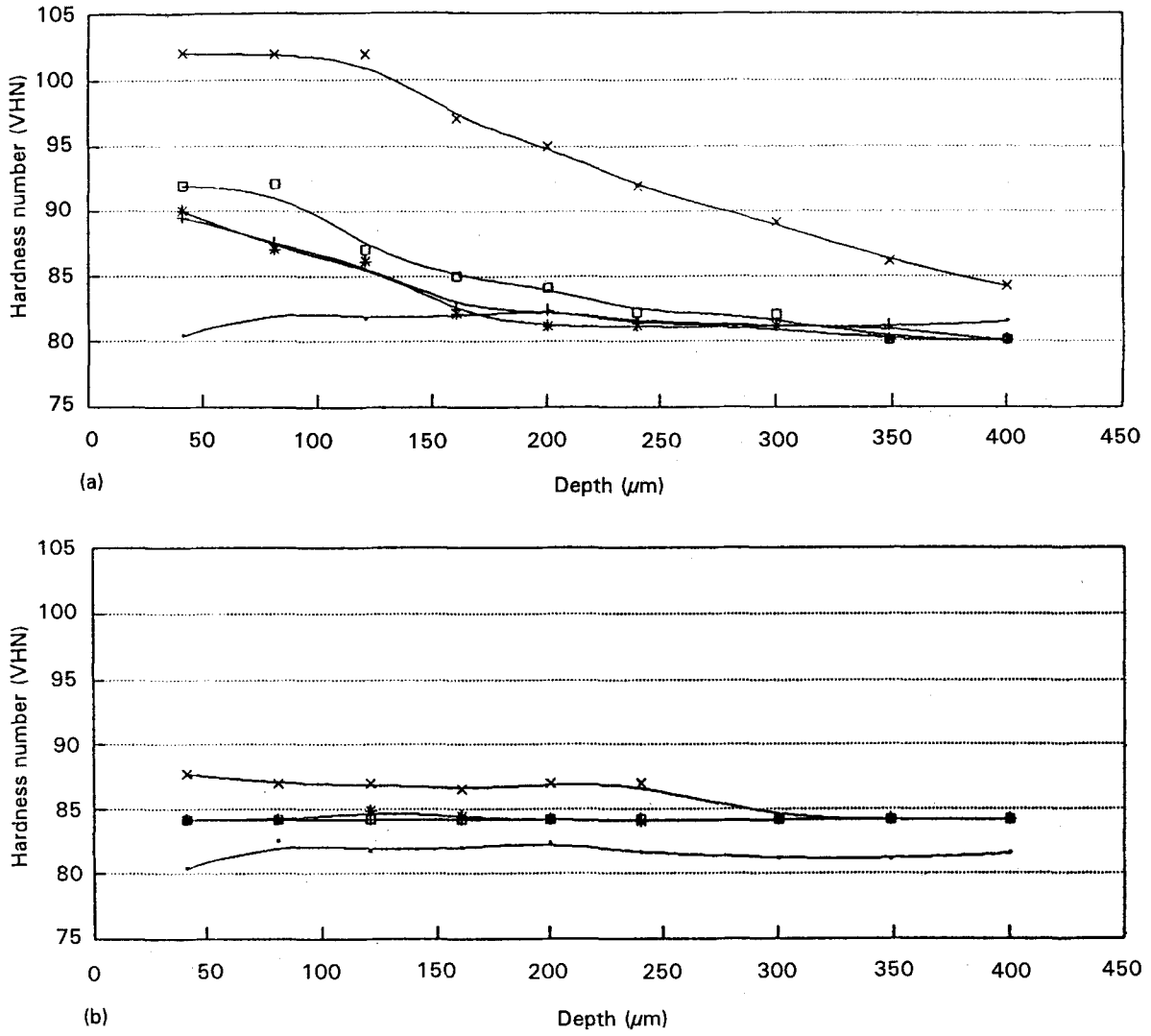

Figure 7 Microhardness (HV 50 G) profiles of alloy 8090-T851 (a) charged at differing current densities, and (b) charged and then degassed (443 K for 1 h). (——) Uncharged, (+) 2 mA cm^{-2}, (*) 4 mA cm^{-2}, (□) 6 mA cm^{-2}, (×) 10 mA cm^{-2}.

and interpretation of hydrogen effects on deformation behaviour of the alloy.

Owing to the similar welding parameters used, bulk composition of the weld metal remained the same for all of the specimens which were charged at the different charging current densities resulting in differing amounts of hydrogen in the welds. Because the Al–Li–Cu–Mg–Zr alloy 8090 is precipitation hardenable, welding results in loss of an intrinsic amount of strengthening in the weld metal. Consequently, all of the specimens were found to fail in the region of the weld metal. However, it is possible to increase the strength of the weld metal by post-weld heat treatment [43].

3.4. Hardness measurements

Vicker's hardness measurements and resultant profiles of both the charged weld and the base metal (8090-T6), measured across the thickness, are illustrated in Fig. 8. An increase in hardness of the charged over uncharged weld metal and base metal was observed. Hardness profiles of the alloy 8090-T851 (Fig. 7a) show an increase in hardness closer to the outer surface. This is attributed to intrinsic differences in hydrogen densities across the thickness of the specimen. More nascent hydrogen will diffuse at the outer surface than at the centre, thereby, resulting in a higher hardness at the outer surface of the specimen. Although the hydrogen diffusion coefficients across the thickness of the specimen were not experimentally measured, the shape of hardness profile indirectly explains the distribution of hydrogen in the matrix. Besides, an increase in charging current density shifts the hardness profile to a higher value and the average hardness of the inner surface increases (Fig. 7a). The hardness profile of the uncharged specimen shows an initial drop in the hardness at the outer surface in comparison with hardness at the centre (Fig. 7b). This degradation is attributed to lithium depletion at the outer surface, resulting in lower hardness values [37].

3.5. Fractography

To understand the fracture mode and to characterize the microscopic fracture features, all deformed samples were examined in a scanning electron microscope. Extensive fractography of the tensile fracture surfaces

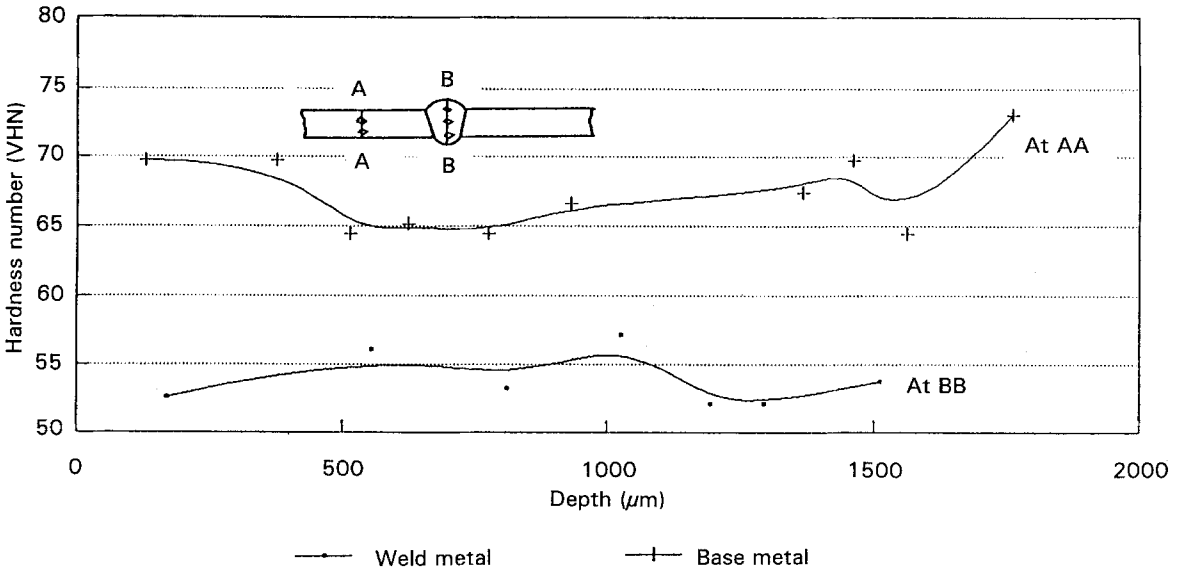

Figure 8 Microhardness (HV 50 G) profiles of charged GTAW weld measured at different locations.

revealed a typical mixed mode of failure with extensive shear-dominated planar slip (Fig. 9). Similar observations have been reported by other investigators [44, 45]. Representative fracture features of the sample are shown in Figs 9–13.

Although, the uncharged specimen welds exhibited a mixed mode or bimodal failure, macroscopic fracture was characterized by the presence of large population of dimples (Fig. 10). Microvoid growth and coalescence resulted in extensive secondary cracking (Fig. 11). The dimple-like features indicate ductile failure. Even though the fracture features of the charged weld specimens were similar to those of uncharged counterpart, some contrasting features were identified at and near the outer surface. From the outer surface up to a certain depth, the fracture mode was predominantly shear dominated planar slip (Fig. 12). This is characteristic of the quaternary 8090 alloy. However, the inner surface was characterized by presence of dimples (Fig. 13). The change in fracture mode is attributed to an intrinsic variation of hydrogen content across the thickness of the charged welds, as indicated by hardness measurements. More hydrogen tends to diffuse into the lattice at and near the outer surface than at the centre. As a result, the fracture at the surface edges was extensive planar slip while subsequent fracture was characterized by overload failure. The overload region was characterized by the presence of features reminiscent of ductile failure, that is,

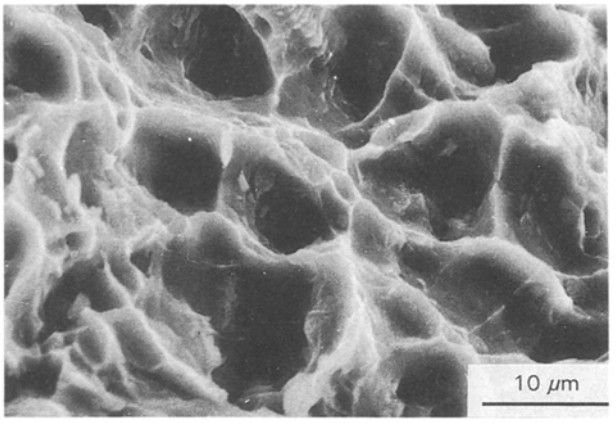

Figure 10 Scanning electron micrograph of tensile fracture surface of uncharged welds showing a large population of dimple features.

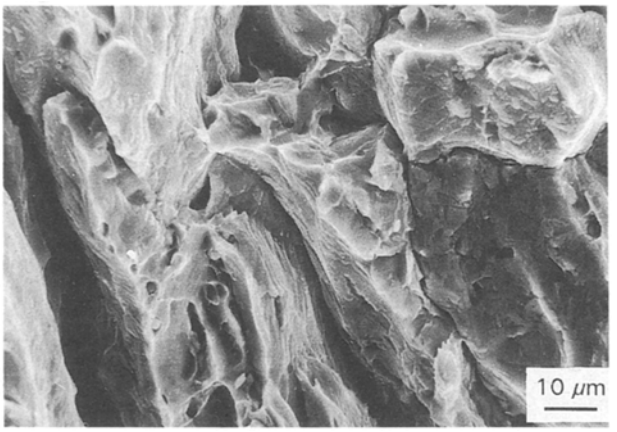

Figure 11 Scanning electron micrograph of tensile fracture surface of the uncharged welds showing secondary cracking.

Figure 9 Scanning electron micrograph of tensile fracture surface of alloy 8090 showing typical mixed mode of failure.

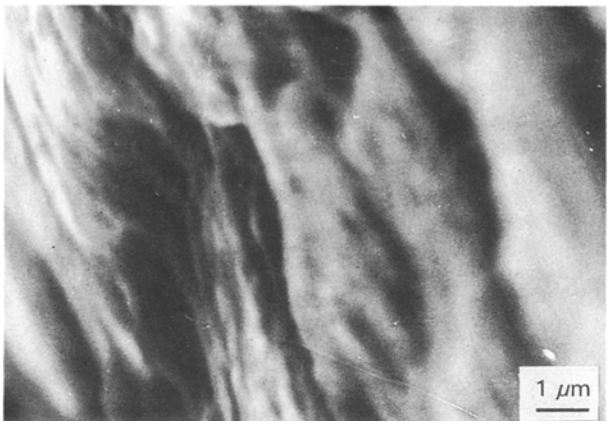

Figure 12 High-magnification scanning electron micrograph of the tensile fracture surface of the charged welds indicating extensive planar slip deformation near the outer surface of the specimen.

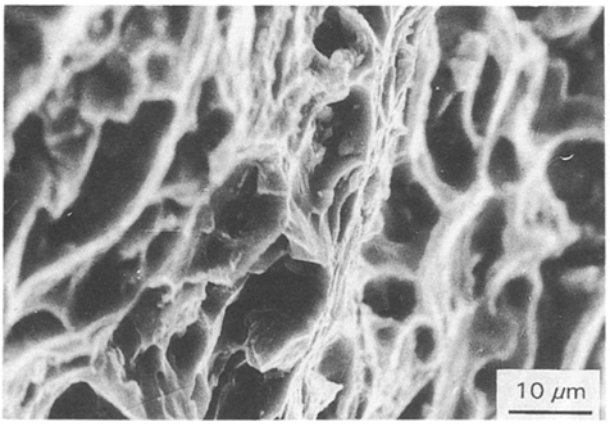

Figure 13 Scanning electron micrograph of tensile fracture surface of uncharged welds showing shallow dimples at the central portion of the weld.

dimples and voids. The change in microscopic fracture mode observed across the thickness is to be expected based on hardness measurements through the thickness of the charged welds (Fig. 8).

4. Conclusions

Based on the results of the present investigation on Al–Li alloy 8090-T6 welds the conclusions are summarized as follows.

1. The effect of cathodic hydrogen charging on ductility parameters of GTAW welds of the aluminium–lithium 8090 is recognized through a decrease in both per cent reduction in area and elongation-to-failure.

2. Extensive microscopic analysis revealed grain coarsening in the weld metal. The change in grain morphology is attributed to intrinsic differences in the rate of cooling of the weld metal during solidification.

3. The observed decrease in ductility of the welds due to charging is attributed to the formation and presence of high-pressure H_2 gas in the fine micropores. The trapped hydrogen gas causes localized deformation to occur. Hardness measurements of welds, at different locations, revealed an increase in hardness due to hydrogen charging. However, degassing of the charged specimens restored the hardness to that of the uncharged alloy. Degassing has a favourable effect as it tends to remove the hydrogen gas from the micropores present in the charged specimens.

4. Scanning electron microscopy observations of uncharged welds revealed a mixed mode or bimodal failure with predominantly ductile rupture. Even though the fracture mode of the charged welds was similar to that of the uncharged counterpart, extensive planar slip deformation was observed at and near the outer surface of the charged weld specimens.

Acknowledgements

The authors thank the Materials Panel, Aeronautical Research and Development Board, Government of India (Research Grant Aero/RD-134/100/10/89-90/581) and Aeronautical Development Agency (Research Grant 612/05/88) for providing financial support. The welding facility extended by Hindustan Aeronautics Limited (HAL), Bangalore, India, and the technical assistance of Mr J. Chandrashekar, Welding Engineer, Aerospace Division, HAL, are gratefully acknowledged.

References

1. E. S. BALMUTH and R. SCHMIDT, in "Aluminum–Lithium Alloys", Proceedings of the First International Conference, edited by T. H. Sanders Jr and E. A. Starke Jr (TMS-AIME, Warrendale, PA, 1981) p. 69.
2. E. A. STARKE Jr and T. H. SANDERS Jr (eds), "Aluminum–Lithium Alloys II", Proceedings of the Second International Conference (TMS-AIME, Warrendale, PA, USA, 1984).
3. C. BAKER, P. J. GREGSON, C. J. PEEL and S. J. HARRIS (eds), "Aluminum–Lithium Alloys III", Proceedings of the Third International Conference (Institute of Metals, London, 1985).
4. C. CHAMPION, D. DUBOST, S. D. MIANNAY and L. SABETAY (eds), "Aluminum–Lithium IV", Proceedings of the Fourth International Conference (Les Editions de Physique, Paris, France, 1987).
5. T. H. SAUNDERS Jr and E. A. STARKE Jr (eds), "Aluminum–Lithium V", Proceedings of the Fifth International Conference (Materials and Component Engineering Publications, Birmingham, UK, 1989).
6. "Aluminum–Lithium VI": Deutsche Gesellschaft fur Materialkunde (Garmisch Partenkirchen, FRG, 1991).
7. T. H. SANDERS Jr and E. S. BALMUTH, *Met. Progr.* **113** (1978) 32.
8. R. E. LEWIS, D. WEBSTER and I. G. PALMER, AFML Technical Report AFML Contract F33615-77-C-5186, Air Force Materials Laboratory, OH, USA, July 1978.
9. E. A. STARKE Jr, T. H. SANDERS Jr and I. G. PALMER, *J. Metals* **12** (1981) 24.
10. P. J. GREGSON and H. M. FLOWER, *Acta Metall.* **33** (1985) 527.
11. T. S. SRIVATSAN and E. J. LAVERNIA, *J. Mater. Sci.* **26** (1991) 940.
12. J. R. PICKENS, *ibid.* **20** (1983) 4247.
13. J. R. PICKENS, F. H. NEUBAUM, T. J. LANGAN and L. S. KRAMER, in "Aluminum–Lithium Alloys V", Proceedings of Fifth International Conference, edited by E. A. Starke Jr and T. H. Sanders Jr (Materials and Component Engineering Publications, Birmingham, UK, 1989) p. 1397.
14. R. J. RIOJA and R. H. GRAHAM, *Adv. Mater. Proc.* **6** (1992) 23.

15. C. E. CROSS, D. L. OLSON, G. R. EDWARDS and J. F. CAPES, in "Aluminum–Lithium II", edited by E. A. Starke Jr and T. H. Sanders Jr (TMS-AIME, Warrendale, PA, 1984) p. 675.
16. T. S. SRIVATSAN and T. S. SUDARSHAN, *Weld. J.* **7** (1991) 173.
17. P. A. MOLIAN and T. S. SRIVATSAN, *J. Mater. Sci.* **25** (1990) 3347.
18. *Idem, Mater. Lett.* **9** (7–8) (1990) 245.
19. *Idem, Aluminium Int. J.* **66** (1990) 69.
20. M. R. EDWARDS and V. E. STONEHAM, in "Aluminum–Lithium Alloy IV", edited by G. Champier, B. Dubost, D. Miannay and L. Sabetay (Institute of Metals, Paris, France, 1987) c3-293.
21. Le POAC, A. M. NOMINE and D. MIANNAY, *ibid.* c3-301.
22. L. S. KRAMER, F. H. HEUBAUM and J. R. PICKENS, in "Aluminum–Lithium V", edited by T. H. Sanders Jr and E. A. Starke Jr (Materials and Component Engineering Publication, Oxford, UK, 1990) pp. 1415–21.
23. J. W. WATSON, Y. Z. SHEN and M. MESHII, *Metall. Trans.* **19A** (1988) p. 2299.
24. R. BALASUBRAMANIAM, D. J. DUQUETTE and K. RAJAN, *Acta Metall. Mater.* **39** (1991) 2597.
25. *Idem, ibid.* **39** (1991) 2607.
26. *Idem*, in "Aluminum–Lithium V", edited by T. H. Sanders Jr and E. A. Starke Jr (Materials and Component Engineering Pulications, Oxford, UK, 1989) pp. 1261–6.
27. D. P. HILL, D. B. WILLIAMS and C. E. MOBLEY, in "Aluminum–Lithium Alloys II", edited by E. A. Starke Jr and T. H. Sanders Jr (TMS-AIME, Warrendale, PA, 1984) pp. 201–11.
28. E. J. LAVERNIA, T. S. SRIVATSAN and F. A. MOHAMED, *J. Mater. Sci.* **25** (1990) 1137.
29. E. NESS and N. RYUM, *Scripta Metall.* **5** (1971) 987.
30. R. J. RIOJA and E. A. LUDWICZAK, in Proceedings of the Third International Conference on Aluminum–Lithium Alloys, "Aluminum–Lithium Alloys III", edited by C. Baker, P. J. Gregson, S. J. Harris and C. J. Peel (Institute of Metals, London, 1985).
31. J. M. GALBRAITH, M. H. TOSTEN and P. R. HOWELL, *J. Mater. Sci.* **22** (1987) 27.
32. R. E. CROOKS and E. A. STARKE Jr, *Metall. Trans.* **15A** (1984) 1367.
33. A. Ya. ISHCHENKO and A. G. CHAYUN, in "International Conference on Aluminum Weldments – II", Munich, FRG, May 1982, I10.1.
34. U. KRUEGER, *Aluminium* **60** (1984) s831.
35. J. R. PICKENS, Technical Information, Martin-Marietta Laboratory, Baltimore, USA.
36. J. R. PICKENS, *J. Mater. Sci.* **25** (1985) 4247.
37. S. MRADULLA and E. S. DWARAKADASA, *J. Mater. Sci. Lett.* **11** (1992) in press.
38. M. J. BULL and D. J. LLOYD, in "Aluminum–Lithium Alloy III", edited by C. Baker, P. J. Gregson, S. J. Harris and C. J. Peel (Institute of Metals, Oxford, UK, 1986) pp. 402–10.
39. P. K. MAKIN and W. M. STOBBS, *ibid.* pp. 392–8.
40. A. RAVINDRA, RAJAN AMBAT and E. S. DWARAKADASA, in "International Conference on Aluminum (INCAL-91)", edited by E. S. Dwarakadasa, S. Seshan and K. P. Abraham, Bangalore, India, July 1991, (Aluminum Association of India) pp. 929–935.
41. A. RAVINDRA, MTech thesis, Indian Institute of Technology, Madras, India (1990).
42. AMIT BANDYOPADHYAY, ME thesis, Department of Metallurgy, Indian Institute of Science, Bangalore, India (1992).
43. A. RAVINDRA and E. S. DWARAKADASA, *J. Mater. Sci. Lett.* **11** (1992) in press.
44. T. S. SRIVATSAN and T. ALAN PLACE, *J. Mater. Sci.* **24** (1989) 1543.
45. T. S. SRIVATSAN, T. A. PLACE and T. S. SUDARSHAN, in "Advances in Fracture Research", Proceedings of the Seventh International Conference on Fracture (ICF-7), edited by P. Rama Rao, K. Salama, K. Ravi-Chandar, and D. M. R. Taplin (Pergamon Press, New York, 1989) pp. 2611–21.

Received 28 July 1992
and accepted 31 August 1993